Superconducting Pairing through the Spin Resonance Mode in High-Temperature Cuprate Superconductors

F. Onufrieva and P. Pfeuty
Laboratoire Léon Brillouin CE-Saclay, 91191 Gif-sur-Yvette, France
(Received 21 February 2008; published 22 May 2009)

We find that the spin resonance mode mediator scenario can explain important anomalies observed in the superconducting (SC) high-T_c cuprates: the famous low energy nodal kink with its doping dependence, the U-shaped form of the SC gap angular dependence, the anomalous form of electron density of states, the high absolute value of the SC gap, and some other unconventional properties.

DOI: 10.1103/PhysRevLett.102.207003 PACS numbers: 74.20.Rp, 74.20.Mn, 74.72.−h

After 20 years of intense research the mechanism of superconductivity in the high-T_c cuprates is still unknown. The observed structure of the low energy electron spectrum is often considered as a signature of a strong electron coupling to some boson, which then is suspected to be a mediator of the SC pairing. If so, possible candidate bosons should be submitted to the following tests: First, an explicit relation between the electron spectrum anomalies (such as the nodal kink [1–4] position, the tunneling density of states (DOS) anomaly [5–7] positions,...) and the boson characteristics should be established. Second, the candidate boson should provide the features of the SC pairing known from experiment: the order-parameter symmetry (nodes, sign change in the Brillouin zone (BZ)), the deviation from the d-wave form in the SC gap angular dependence (the so called U-shaped form [8–10]), its high absolute value. Third, the same scenario should be able to explain other unconventional properties of the high-T_c cuprates, or at least some of them. Here we consider the famous spin resonance mode (SRM) as a candidate boson. We ask the following questions: Would features of the mediated SC state have something similar to the anomalies observed in the high-T_c cuprates? If so we will submit the spin resonance mode to the tests formulated above. The results are discussed in the end of the Letter.

Strong antiferromagnetic spin fluctuations in the superconducting cuprates have been discovered quite early. Their most prominent and intense feature is the resonance peak, seen by neutron at wave vector $\mathbf{Q} = (\pi, \pi)$ [11,12]. A possible theoretical explanation was provided early in [13,14]. Later on it was shown [15] that more generally a resonance collective mode with a slight downward dispersion $\omega_{\mathbf{p}}$ should develop in the d-wave type SC state. Such a mode indeed was observed experimentally, first in [16] and later in a number of neutron experiments. Its properties are imposed by its nature [15]: Being a bound state exciton mode it develops inside the gap in the electron-hole continuum. Since this gap area is limited not only in energy but also in momentum, the mode is characterized by the ending wave vector $\mathbf{q}_{\text{end}}$, where it approaches the electron-hole continuum and its intensity becomes negligible. The mode should be coupled strongly to the electron system since its existence in itself is a signature of strong electron-spin coupling. From a microscopic point of view, such a coupling is present in the t-J model, the most adequate model for the low energy physics of the CuO_2 plane. Despite the presence of this microscopic background, we will stay on a more phenomenological level using in the calculations the characteristics observed experimentally for SRM and a phenomenological parameter for its interaction with electrons. For bare electrons corresponding effectively to the CuO_2 plane, the spectrum is $\epsilon^0_{\mathbf{k}\sigma} = -2t(\cos k_x + \cos k_y) - 4t' \cos k_x \cos k_y - \mu$ with a saddle point (SP) at $\mathbf{k} = (0, \pi)$.

Overview of the formalism.—In the SC state the electron Green function $\hat{G}$ is a 2×2 matrix with the diagonal (Normal) component G^N describing off-condensate electrons and the off-diagonal (Anomalous) component G^A describing pairing correlations. The Dyson equation relates them to the self-energies Σ^N, Σ^A:

$$G^N(\mathbf{k}, \Omega) = \frac{\Omega + e_{\mathbf{k}}(-\Omega)}{D(\mathbf{k}, \Omega)}, \qquad G^A(\mathbf{k}, \Omega) = \frac{\Sigma^A_{\mathbf{k}}(\Omega)}{D(\mathbf{k}, \Omega)},$$
$$D(\mathbf{k}, \Omega) = [\Omega - e_{\mathbf{k}}(\Omega)][\Omega + e_{\mathbf{k}}(-\Omega)] - |\Sigma^A_{\mathbf{k}}(\Omega)|^2, \tag{1}$$

$e_{\mathbf{k}}(\Omega) = \epsilon^0_{\mathbf{k}} + \Sigma^N_{\mathbf{k}}(\Omega)$. The self-energy due to electron-spin exchange is given by $\hat{\Sigma} = \hat{\Gamma}^0 \hat{G} \hat{K} \hat{\Gamma}$ (where $\hat{K}$, $\hat{\Gamma}$ and $\hat{\Gamma}^0$ are the spin Green function, full and bare vertices) or explicitly for its components by

$$\Sigma^{N,A}_{\mathbf{k}}(\Omega) = -\frac{3\tilde{g}^2}{4N} \sum_{\mathbf{p}} \iint \frac{d\omega}{\pi} \frac{d\epsilon}{\pi} \operatorname{Im} G^{N,A}(\mathbf{p} + \mathbf{k}, \epsilon) \times \operatorname{Im} K(\mathbf{p}, \omega) \frac{\coth(\omega/2T) + \tanh(\epsilon/2T)}{\omega + \epsilon - \Omega - \operatorname{sgn}(\Omega) i\delta}, \tag{2}$$

where we introduced the effective interaction $\tilde{g}^2 \hat{I} = \hat{\Gamma} \hat{\Gamma}^0$. The boson propagator is taken in the form chosen to best reproduce the SRM properties, $\operatorname{Im} K(\mathbf{q}, \omega) = a_{\mathbf{q}} \delta(\omega - \omega_{\mathbf{q}})$, $a_{\mathbf{q}} = A[1 - b(q_x^2 + q_y^2)]\theta(q^\phi - q^\phi_{\text{end}})$, $\mathbf{q} = \mathbf{Q} - \mathbf{p}$, $\mathbf{q}_{\text{end}} = q^\phi_{\text{end}} \mathbf{n}$, $\phi = 0$ stands for the direction (1,0), we neglect the SRM weak dispersion, $\omega_{\mathbf{q}} = \omega_r$. The spin-electron coupling is characterized by $\Lambda = \frac{1}{N} \frac{3\tilde{g}^2}{2\omega_r} \sum_{\mathbf{q}} a_{\mathbf{q}}$.

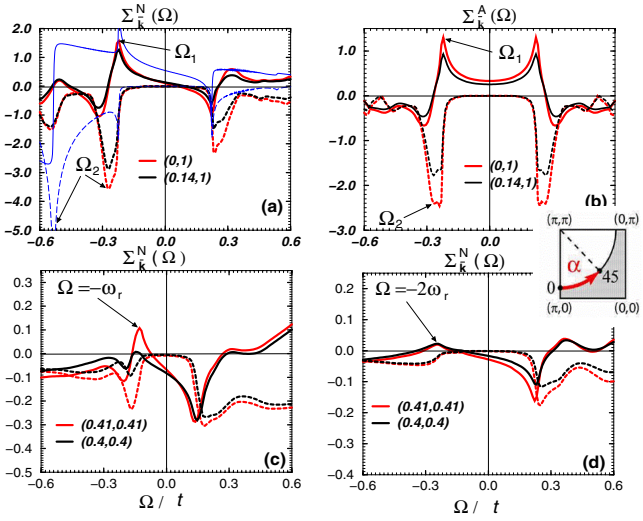

FIG. 1 (color online). Self-energies for different $\bar{\mathbf{k}} = \mathbf{k}/\pi$ in the antinodal (a), (b), and nodal (c), (d) regions. Solid lines correspond to $t\mathrm{Re}\Sigma^{N,A}$, dashed lines to $-|t\mathrm{Im}\Sigma^{N,A}|$, blue lines in (a) to the non-self-consistent $\Sigma^{N}_{(0,\pi)}$ calculated with imposed d-wave gap. In (c) $q_{\mathrm{end}} = 0.32$. Note that the form of Ω dependences depends much on $\mathbf{k}$ and q_{end}, compare (a) and (c), (c) and (d). Inset shows the schematical FS.

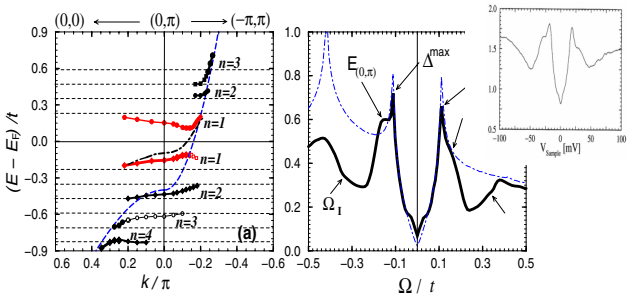

FIG. 2 (color online). Electron spectrum near (0, π) (a) and electron DOS (b). In (a) black lines correspond to unpaired electron spectrum $\tilde{\epsilon}_{\mathbf{k}}$; for the paired electron spectrum, the branch $n = 1$ (black dashed line) splits into two (red lines), the high energy branches are practically unchanged. Calculated $\lambda^{\alpha=0} = 1.2$. Blue lines correspond to the bare spectrum in (a) and to the BCS DOS in (b). Inset shows tunneling data [5].

Equations (1) and (2) represent a couple of nonlinear integral equations that is difficult to resolve. The often used simplification consisting to neglect the self-energy momentum dependence (or to impose a momentum-energy factorization keeping the same energy form for all wave vectors), see, for example, [17] being justified in the case of isotropic electrons and s-wave pairing is not justified for the cuprates given the high anisotropy of the observed electron Fermi surface (FS) and of the SC gap. Another simplification, the linearization of the equations (supposing the SC gap, $\Delta \to 0$) is relevant only near T_c. Such approximation was used in [18], where spin fluctuations were probed for SC pairing in the cuprates for the first time. The fluctuations themselves were taken of relaxation type that is also relevant only near T_c. The equations similar to (1) and (2) with a resonance spin propagator were considered in [19]. But they were not solved self-consistently and the problem of SC pairing was not treated.

We solve the equations on the real axis using the parameters: For electrons: $t'/t = -0.3$, $\epsilon^{0}_{(0,\pi)} = -0.4t$ (to get the FS similar to that observed by ARPES). For SRM: The ImK 2D $\mathbf{q}$-distribution is taken of diamond form [15,20], $q^{\phi}_{\mathrm{end}} = q_{\mathrm{end}}(\cos\phi + \sin\phi)^{-1}$. The energy is taken $\omega_r = 0.12t$ (the observed $\omega_r \sim 30$–40 meV depending on doping and $t \sim 300$ meV). For q_{end} we probe two values, low and intermediate, giving a qualitatively different electronic behavior as we will see ($q_{\mathrm{end}} = 0.22$ if not specified). The interaction is taken $\tilde{g} = 4t$.

The obtained self energies (important examples are presented in Fig. 1) allow calculation of different observable properties: For example the renormalized electron spectrum is given by Eq. $\Omega = \pm E_{\mathbf{k}}(\Omega) \equiv \pm\sqrt{\tilde{\epsilon}^2_{\mathbf{k}}(\Omega) + \Delta^2_{\mathbf{k}}(\Omega)}$ when quasiparticles are well defined [$\tilde{\epsilon}_{\mathbf{k}}(\Omega) = (\epsilon^0_{\mathbf{k}} + \Sigma^{+}_{\mathbf{k}\Omega})/Z_{\mathbf{k}}(\Omega)$, the energy dependent SC gap is $\Delta_{\mathbf{k}}(\Omega) = |\Sigma^{A}_{\mathbf{k}}(\Omega)|/Z_{\mathbf{k}}(\Omega)$, the renormalization factor is $Z_{\mathbf{k}}(\Omega) = 1 - \Sigma^{-}_{\mathbf{k}\Omega}/\Omega$, $\Sigma^{\pm}_{\mathbf{k}\Omega} = (\Sigma^{N}_{\mathbf{k}}(\Omega) \pm \Sigma^{N}_{\mathbf{k}}(-\Omega))/2$]. Otherwise, the electron "spectrum" is determined by peaks of the spectral functions $A(\mathbf{k}, \Omega) = |\mathrm{Im}G^{N}(\mathbf{k}, \Omega)|$ as a function of Ω for fixed $\mathbf{k}$ [energy distribution curves (EDC's)]. The electron DOS is determined by $N(\Omega) = \frac{1}{N}\Sigma_{\mathbf{k}}|\mathrm{Im}G^{N}(\mathbf{k}, \Omega)|$. The SC gap in the direction α is given by $\Delta^{\alpha} \equiv \Delta^{\alpha}_{\mathbf{k}_F}(\Omega = \Delta^{\alpha}_{\mathbf{k}_F})$, the spectrum by $E_{\mathbf{k}} \equiv E_{\mathbf{k}}(\Omega = E_{\mathbf{k}})$, $\tilde{\epsilon}_{\mathbf{k}} \equiv \tilde{\epsilon}_{\mathbf{k}}(\Omega = \tilde{\epsilon}_{\mathbf{k}})$. In a close vicinity of ϵ_F one can present $\tilde{\epsilon}_{\mathbf{k}} = v^{\alpha}_{F}(k - k^{\alpha}_{F})/(1 + \lambda^{\alpha})$, the form that introduces the dimensionless electron-spin coupling $\lambda^{\alpha} = Z_{k^{\alpha}_{F}}(0) - 1$, similar to the electron-phonon case but angle dependent (the azimuthal angle α is determined in the inset of Fig. 1).

Renormalized electron spectrum.—Its most important feature is a fractionalization whatever is the direction in the BZ. [The typical spectrum looks like in Fig. 2(a).] The fractionalization appears already in the unpaired electron spectrum $\tilde{\tilde{\epsilon}}_{\mathbf{k}}$ obtained when calculating $A(\mathbf{k}, \Omega)$ with $\Sigma^{A} = 0$, black lines. [In the paired electron spectrum a splitting of the low energy branch occurs in addition (red lines).] To understand the effect let us remind that in the self consistent calculations the renormalized spectrum is determined by the self-energies that in turn are determined by this spectrum. The low energy part of the spectrum given by $E_{\mathbf{k}}$ with $\tilde{\epsilon}_{\mathbf{k}} = v^{\alpha}_{F}(k - k^{\alpha}_{F})/(1 + \lambda^{\alpha})$ and Δ^{α}, produces sharp peaks in $\mathrm{Re}\Sigma^{N,A}$ and $\mathrm{Im}\Sigma^{N,A}$ near $\Omega = \pm\Omega_1 = \mp(\omega_r + \Delta^{\alpha})$; see Figs. 1(a)–1(c). As a result, the energies $\pm\Omega_1$ turn out to be ending points in the low energy coherent electron spectrum: the branch $n = 1$ is formed. The pseudogap above the branch $n = 1$ appears being related to the high value of $|\mathrm{Im}\Sigma^{N,A}|$. Above the pseudogap, coherent electrons reappear forming second branch ($n = 2$ satellite). This branch forms high energy

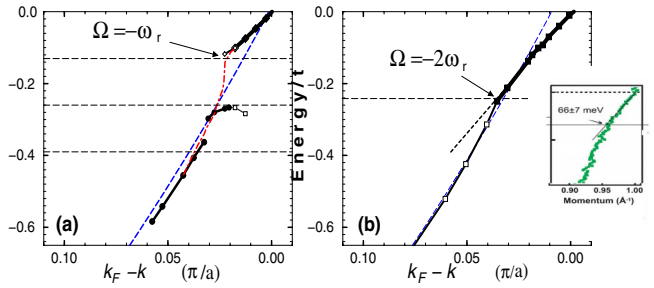

FIG. 3 (color online). Electron spectra in the nodal direction. $q_{\rm end} = 0.32$ in (a), 0.22 in (b). Calculated $\lambda^{\alpha=\pi/4} = 1.1$ in (a), 0.65 in (b). Red lines in (a) correspond to momentum distribution curves (MDC's). Inset shows ARPES data for YBCO [4].

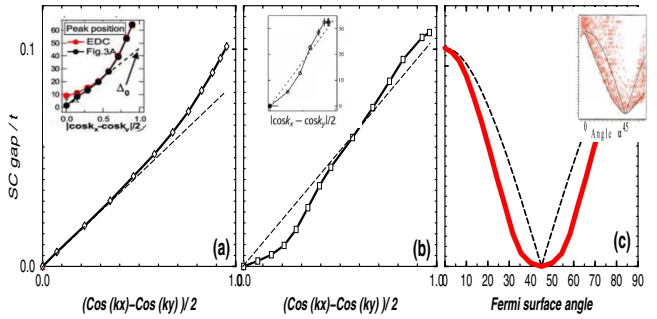

FIG. 4 (color online). SC gap Δ^{α} along the renormalized FS. In (a) $q_{\rm end} = 0.32$, in (b), (c) 0.22. Dashed lines correspond to the d-wave gap, $\Delta_{\mathbf{k}} = \Delta(\cos k_x - \cos k_y)/2$. [When calculating we added a small next-next-nearest-neighbor hopping $t''/t = 0.015$ to better reproduce the experimental FS]. The insets shows ARPES data: [25] (a), [9] (b), [10] (c).

maxima in $|{\rm Im}\Sigma^{N,A}|$, $|{\rm Re}\Sigma^{N,A}|$, which in turn produce new pseudogaps and so on. The satellite intensity decreases with increasing n. Stronger is the coupling and closer is the direction to the antinodal one, higher is the number of visible satellites. The satellites and pseudogaps are located approximately within the energy bands $m\omega_r + \Delta^{\alpha} < |\Omega| < (m+1)\omega_r + \Delta^{\alpha}$ with $m = 2, 4, \ldots$ and $m = 1, 3, \ldots$ respectively. We emphasize the difference with the non self-consistent calculations in which only splitting into two branches occurs: for the parameters we use, the high energy branch corresponds approximately to the $n = 4$ branch in Fig. 2(a), the low energy branches $n = 2, 3$ are missing.

Nodal direction.—In the case of intermediate $q_{\rm end}$ value, the spectrum exhibits the common for any direction features, see in Fig. 3(a) the fractionalized branches and pseudogaps separated by the lines $|\Omega| = m\omega_r + \Delta^{\alpha}$ with $\Delta^{\alpha} \ll \Delta^{\max} \equiv \Delta^{\alpha=0}$. We found, however, a surprisingly different behavior [Fig. 3(b)] for a slightly lower $q_{\rm end}$ value: there is no pseudogap above $|\Omega| = \omega_r$, but a pronounced kink at $\Omega = -2\omega_r$. The reason for this is a very different behavior of the corresponding self-energies [see Figs. 1(c) and 1(d)], namely, the absence of the main peak at $\Omega \sim \Omega_1 = -\omega_r$ in the case $q_{\rm end} = 0.22$. The analysis shows that the behavior in Fig. 1(c) [and therefore that in Fig. 3(a)] takes place when $q_{\rm end}^{\phi=\pi/4} > |\mathbf{q}_m^{\alpha=\pi/4}| + \omega_r/v_F^{\alpha=\pi/4}$ (where $\pi\mathbf{q}_m^{\alpha=\pi/4} = \mathbf{Q} - 2\mathbf{k}_F^{\alpha=\pi/4}$) and the behavior in Figs. 1(d) and 3(b) does it in the opposite case. The reason is the absence in the latter case of the effective interaction between the FS electrons and electrons with wave vectors corresponding to the presumed pseudogap. As a consequence the satellite peak at $\Omega \sim -2\omega_r$ becomes a dominant feature in ${\rm Re}\Sigma^{N}$ [Fig. 1(d)]. Note that if the spin mode has a purely itinerant origin and corresponds to the resonance mode below the electron-hole continuum, then necessarily $q_{\rm end}^{\phi=\pi/4} < |\mathbf{q}_m^{\alpha=\pi/4}| + \omega_r/v_F^{\alpha=\pi/4}$ and the scenario corresponding to Fig. 3(b) takes place. This scenario corresponds well to the experimental data for $YBa_2Cu_3O_{6+x}$ (YBCO); compare the kink energies observed by ARPES [4], $\Omega_{\rm kink} = 66 \pm 7$ meV, 78 ± 5 meV for $T_c = 61$, 90 K, respectively, and the SRM energies observed by neutron, $\omega_r = 34$ [20], 41 meV [11] for $T_c = 63$, 91 K, respectively. For $Bi_2Sr_2CaCu_2O_{8+\delta}$ (BSCO) the situation is less clear: the spin dynamics is much less studied (neutron data exist only for over- and optimal doping giving $\omega_r \sim 43$ meV [21]) and there is no consensus on the kink position in ARPES: $\Omega_{\rm kink} = 43$ [2], 50 [1], and 54 mev [3] (all the data are for optimal doping). Still, there is qualitative agreement with our results since the observed mode is quite large in momentum [21] (twice with respect to YBCO) and therefore it is rather the scenario corresponding to Fig. 3(a) that should take place, i.e., the kink should be located slightly above $|\Omega| = \omega_r$. For $La_{2-x}Sr_xCuO_4$ (LSCO) the spin dynamics is rather different [22] while the similar kink is observed in ARPES [1]. There is, however, no contradiction and the kink is well explained by the spin mode scenario [23].

Antinodal direction—The spectrum exhibits an additional feature: the low energy branch possesses a SP at $(0, \pi)$. Its spectral weight $\tilde{z}_{(0,\pi)}$ is much lower and its energy is heavily renormalized with respect to the bare spectrum, $\tilde{z}_{(0,\pi)} \ll z^0_{(0,\pi)}$, $\tilde{\epsilon}_{(0,\pi)} \ll \epsilon^0_{(0,\pi)}$. In fact due to the constraint $|E_{(0,\pi)}| \equiv \sqrt{(\tilde{\epsilon}_{(0,\pi)})^2 + |\Delta_{(0,\pi)}|^2} < \omega_r + \Delta^{\max}$ (where $\Delta^{\max} \approx \Delta_{(0,\pi)}$) the renormalized $|\tilde{\epsilon}_{(0,\pi)}|$ is of the order of ω_r and therefore is quite small whatever is the bare $|\epsilon^0_{(0,\pi)}|$. The effect is well seen in the self-energies, compare the strength and the position of the "logarithmic singularity" in $\Sigma^{N,A}$ at $|\Omega| = |\Omega_2| = |E_{(0,\pi)}| + \omega_r$ for the self consistent (red) and non self consistent (blue) curves in Fig. 1(a), both due to the SP, in the renormalized and bare spectrum, respectively.

Electron DOS.—There is the same effect in the electron DOS [Fig. 2(b)] which features for $|\Omega| > \Delta^{\max}$ are dominated by the antinodal spectrum: Because of the smallness of $|\tilde{\epsilon}_{(0,\pi)}|$, two peaks, at $|\Omega| = \Delta^{\max}$ due to SC gap and at $|\Omega| = |E_{(0,\pi)}|$ due to SP, are always located nearby whatever is the SP energy of noninteracting electrons. Moreover, the latter peak [Van-Hove singularity (VHS) peak] is hardly seen as a result of weakness of $\tilde{z}_{(0,\pi)}$. This explains

well the tunneling spectroscopy observation (non understood until now) concerning a very weak signature of the VHS in the experimental DOS whatever is doping. Other features at $|\Omega| > \Delta^{\max}$, the valley corresponding to the pseudogap, the following peak corresponding to the $n = 2$ satellite and the inflexion point in the part growing towards the satellite peak (at $\Omega = \Omega_I$), are also very close to the experimental ones. Note, however, that this 2D anisotropic theory inflexion point being extremely similar to the "point of maximal slope" in [6] is not located at $|\Omega| = \Omega_1 = \omega_r + \Delta^{\max}$ as supposed in [6] based on the isotropic SC theories of 60th but around $2\omega_r + \Delta^{\max}$. As to the low energy DOS, it departs from the d-wave form as a consequence of the SC gap specific dependence on azimuthal angle that we discuss below.

SC pairing characteristics.—The SC order parameter changes sign across the main diagonal and vanishes at it due to the symmetry imposed by Eq. (2) and given the electron FS form and the SRM propagator momentum structure. The SC gap decreases from the antinodal to nodal direction while the form of its angular dependence deviates from the d-wave one; see Fig. 4. The details of this deviation depend on details of the spin mode characteristics, most importantly on the relation between $\mathbf{q}_{\text{end}}$ and $2\mathbf{k}_F$. When $q_{\text{end}}^{\phi=\pi/4} > |\mathbf{q}_m^{\alpha=\pi/4}|$, the gap is linear as a function of $(\cos k_x - \cos k_y)$ except for a vicinity of the antinodal point where it increases more rapidly [Fig. 4(a)]. When $q_{\text{end}}^{\phi=\pi/4} < |\mathbf{q}_m^{\alpha=\pi/4}|$, the gap is underlinear in the near-nodal region [Fig. 4(b)] that gives the U-shaped form when the gap is plotted as a function of angle [Fig. 4(c)], the form very close to that observed experimentally [8–10]. Higher is $|\mathbf{q}_m^{\pi/4} - \mathbf{q}_{\text{end}}^{\pi/4}|$, stronger is the deviation from the pure d-wave behavior and larger is the near-nodal region with the reduced gap. Note that both behaviors presented in Figs. 4(a) and 4(b) are observed experimentally in different cuprates, see insets. Both can be considered as a two gap (nodal, antinodal) behavior, the problem discussed intensively in relation with recent Raman and ARPES observations [24,25].

Concluding remarks.—The found features of the SRM mediated SC state are close to those observed experimentally in the cuprates: The SC order parameter changes sign through the main diagonal in the BZ while the SC gap angular dependence is characterized by the U-shaped form as in experiment (the feature not understood until now). The gap value is high: $\Delta^{\max} \sim 0.1t$ ($t \sim 300$ meV) found for relatively low values of electron-spin coupling, $\lambda^{\alpha=0} \sim 1.2$ and $\lambda^{\alpha=\pi/4} \sim 0.65$. The electron spectrum is close to that observed experimentally, both in the antinodal and the nodal regions. In the latter case we deal with an important issue in the high-T_c field since the low energy nodal kink represents the lowest energy scale in the electron dynamics except for the SC gap itself and its origin is presently one of the most controversial point in the debate. We obtain that, quite nontrivially, the kink energy does not necessarily correspond to the mediating boson energy as it is usually supposed. Its position depends on details in the boson momentum structure. We are able to obtain practically exact positions of the nodal kink energy observed by ARPES in YBCO as a function of doping [4] when inputting the SRM energy observed by neutron in YBCO. The electron DOS of the SRM mediated state has an overall form very close to that observed experimentally with multiple peak structure and inflexion point. As in experiment it is characterized by a close location of the gap- and VHS-peaks whatever high is the noninteracting electron SP energy (whatever is doping in experiment) and by the latter peak hardly resolved. The unusual low energy DOS behavior showing up two different gaps, the low- and the high-energy ones, being not seen by tunneling for the moment [except in the data presented in Fig. 2(b)] corresponds well to the observation of two different gaps by other techniques [24,25]. All these results obtained within unified theory constitute an important argument in a favor of the spin mode mediated superconductivity in the high-T_c cuprates.

[1] A. Lanzara *et al.*, Nature (London) **412**, 510 (2001).
[2] T. Sato *et al.*, Phys. Rev. Lett. **91**, 157003 (2003).
[3] A. A. Kordyuk *et al.*, Phys. Rev. Lett. **97**, 017002 (2006).
[4] S. V. Borisenko *et al.*, Phys. Rev. Lett. **96**, 117004 (2006).
[5] I. Maggio-Aprile *et al.*, Phys. Rev. Lett. **75**, 2754 (1995).
[6] J. Lee *et al.*, Nature (London) **442**, 546 (2006).
[7] E. W. Hudson *et al.*, Science **285**, 88 (1999).
[8] J. Mesot *et al.*, Phys. Rev. Lett. **83**, 840 (1999).
[9] D. L. Feng *et al.*, Phys. Rev. Lett. **88**, 107001 (2002).
[10] S. V. Borisenko *et al.*, Phys. Rev. B **66**, 140509(R) (2002).
[11] J. Rossat-Mignod *et al.*, Physica (Amsterdam) **185–189C**, 86 (1991).
[12] H. F. Fong *et al.*, Phys. Rev. B **61**, 14 773 (2000).
[13] F. Onufrieva and J. Rossat-Mignod, Phys. Rev. B **52**, 7572 (1995); F. Onufrieva, Physica (Amsterdam) **251C**, 348 (1995).
[14] I. Mazin *et al.*, Phys. Rev. Lett. **75**, 4134 (1995).
[15] F. Onufrieva and P. Pfeuty, arXiv:cond-mat/9903097; F. Onufrieva and P. Pfeuty, Phys. Rev. B **65**, 054515 (2002).
[16] P. Bourges *et al.*, Science **288**, 1234 (2000).
[17] E. Schachinger *et al.*, Phys. Rev. B **77**, 094524 (2008).
[18] P. Monthoux and D. Pines, Phys. Rev. Lett. **69**, 961 (1992).
[19] M. Eschrig and M. Norman, Phys. Rev. B **67**, 144503 (2003).
[20] S. M. Hayden *et al.*, Nature (London) **429**, 531 (2004).
[21] H. Fong *et al.*, Nature (London) **398**, 588 (1999).
[22] B. Vignolle *et al.*, Nature Phys. **3**, 163 (2007).
[23] In LSCO, Imχ shows two peaks, at $\omega_{r1} \simeq 18$ meV and $\omega_{r2} \simeq 50$ meV [22], that can be modeled by two modes. Calculations (presented elsewhere) show that the nodal spectrum behavior is similar to that in Fig. 3(b) with the kink at the satellite energy $\Omega = -(\omega_{r1} + \omega_{r2})$. This corresponds well to the ARPES data $\Omega_{\text{kink}} \simeq 70$ meV [1].
[24] M. Le Tacon *et al.*, Nature Phys. **2**, 537 (2006).
[25] K. Tanaka *et al.*, Science **314**, 1910 (2006).